Iris Boundaries Segmentation Using the Generalized Structure Tensor.
A Study on the Effects of Image Degradation

Fernando Alonso-Fernandez, Josef Bigun
Halmstad University. Box 823. SE 301-18 Halmstad, Sweden
{feralo, Josef.Bigun}@hh.se

Abstract

We present a new iris segmentation algorithm based on the Generalized Structure Tensor (GST), which also includes an eyelid detection step. It is compared with traditional segmentation systems based on Hough transform and integro-differential operators. Results are given using the CASIA-IrisV3-Interval database. Segmentation performance under different degrees of image defocus and motion blur is also evaluated. Reported results shows the effectiveness of the proposed algorithm, with similar performance than the others in pupil detection, and clearly better performance for sclera detection for all levels of degradation. Verification results using 1D Log-Gabor wavelets are also given, showing the benefits of the eyelids removal step. These results point out the validity of the GST as an alternative to other iris segmentation systems.

1. Introduction

Iris analysis begins with the detection of the inner (pupil) and outer (sclera) boundaries. Its success is crucial for the good performance of iris recognition systems. Although state-of-the-art iris features are very effective for recognition, their performance is greatly affected by iris segmentation [7]. It is reported that most failures to match in iris recognition result from inaccurate segmentation [11]. Several factors can degrade iris images. However, evaluation of its individual effect in the segmentation performance is quite limited [19], with most of the works focused on its impact in the recognition accuracy [10, 16].

Most of the literature bases its core segmentation on the Daugman integro-differential operator [4] or the circular Hough transform, proposed by Wildes [18]. They assume that iris boundaries can be approximated as circles. Newer approaches relax the circularity assumption, but many start with a detector of circular edges, which is further deformed into non-round boundaries. This is the case for example of active contours (also by Daugman) [5], elastic models plus
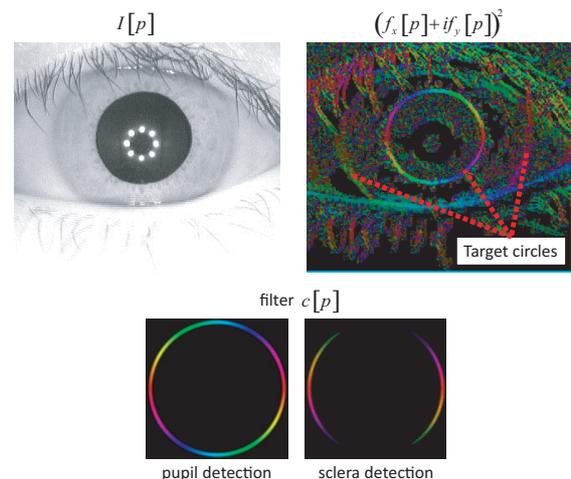

Figure 1. Iris segmentation using the Generalized Structure Tensor (GST). Functions $f_x[p]$, $f_y[p]$ are the partial derivatives of the image $I[p]$ at pixel $p = [x, y]$, and $c(p)$ is a complex circular filter encoding local orientations of the sought pattern. The hue in $(f_x(p) + if_y(p))^2$ and $c(p)$ encodes the direction and the saturation represents the complex magnitude. To depict the magnitude, they are re-scaled so that maximum saturation represents the maximum magnitude and black represents zero magnitude.
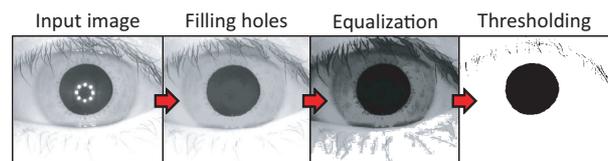

Figure 2. Removal of specular reflections and coarse pupil detection.

spline-based edge fitting [7] or AdaBoost eye detection [8]. Other approaches not relying initially on geometric models for detection, such as Graph Cuts [15], also make use of some circular of elliptical fitting during a refinement stage.

We present a iris segmentation algorithm based on the Generalized Structure Tensor (GST) [1] that also includes an eyelid detection procedure. Apart from a correlation of edge magnitudes, the GST takes into account the direction
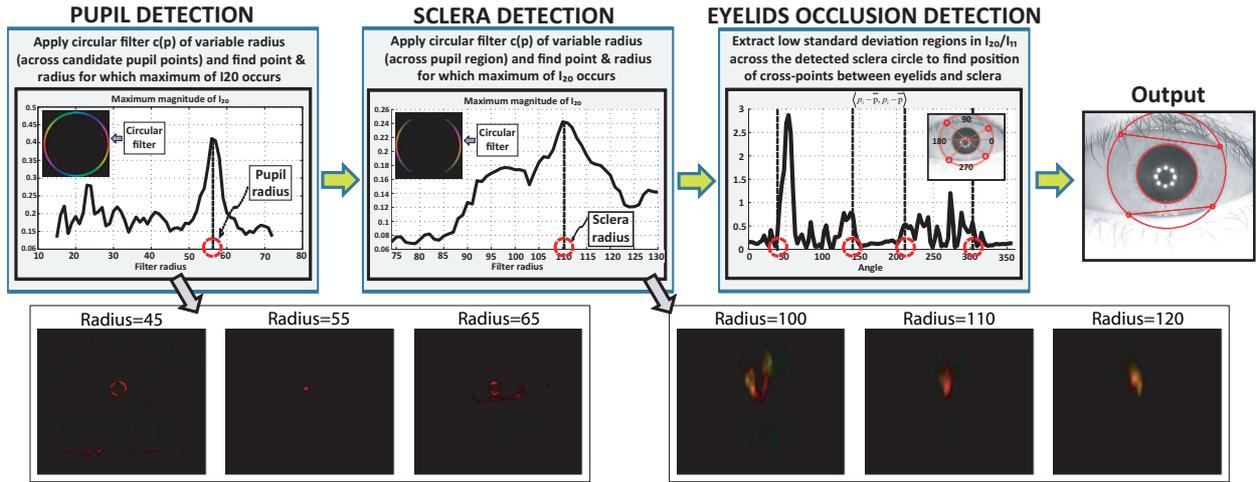
Figure 3. Top: System model for iris segmentation using the Generalized Structure Tensor. Bottom: Tensor I_{20} for different radii of the circular filter $c(p)$. The hue in the images encodes the direction and the saturation represents the magnitude of complex numbers. To depict the magnitude, it is re-scaled so that maximum saturation represents the maximum magnitude of I_{20} and black represents $I_{20} = 0$.

of edges. Thanks to the use of circular complex filters encoding local orientations, its response is penalized if there is disagreement of local orientations of the image with those of the filter. This is not exploited by other edge-based detection methods such as the circular Hough transform or the integro-differential operator, where all boundary pixels contribute equally to (do not penalize) the circle detection. Certain degree of non-circularity can be also accommodated by controlling the filter width, so once approximate circular boundaries are detected, they can be deformed into non-round boundaries. We use for our experiments the CASIA-IrisV3 Interval database, with 2,639 iris images from 249 contributors [3]. Reported results show the effectiveness of the proposed algorithm, outperforming their two counterparts (specially in detecting the sclera boundary). In addition, verification results of the proposed system using 1D Log-Gabor wavelets are given, showing the benefits of the eyelids detection step. We also evaluate the influence of different degrees of image defocus and motion blur in the segmentation performance. Comparatively, our algorithm always gets top performance for all levels of degradation, with similar performance than the others in pupil detection, and clearly better performance for sclera detection.

2. Symmetry Filters and the Generalized Structure Tensor (GST)

Assuming that iris detection can be started with a circular detector [5, 7, 8], it can be done by means of the Generalized Structure Tensor [1]. For this purpose, a circular complex filter $c(p)$ encoding local orientations is used, see Figure 1. Image $(f_x(p) + if_y(p))^2$, built from the estimated partial derivatives $f_x[p]$, $f_y[p]$ of an iris image $I[p]$, is convolved with $c(p)$ as follows:

$$
\begin{aligned}
I_{20} &= \sum_p c(p) \left(f_x(p) + if_y(p)\right)^2 \\
I_{11} &= \sum_p |c(p)| \left|\left(f_x(p) + if_y(p)\right)^2\right|
\end{aligned}
\tag{1}
$$

Magnitudes I_{20} and I_{11} are referred to as the (complex representation of the) structure tensor. It can be shown that a high response in $|I_{20}|$ and zero argument of I_{20} is obtained at a point p if there are edges at the prescribed (same) distance from p and there is an agreement in terms of local orientations (structure tensors) with those of the circle. Also, when this happens, the Schwartz inequality holds with equality ($|I_{20}| = I_{11}$). Since iris boundaries are not exactly round, we can make the width of the filter high enough to allow certain non circularity, and further deform circles into non-round boundaries (the latter is not implemented here).

Filter $c(p)$ is an example of symmetry filters [1], designed to detect points that poses a certain symmetry type (circular, parabolic, linear, etc.). Symmetry filters have been successfully applied to a wide range of detection tasks such as cross-markers in vehicle crash tests [2], core-points and minutiae in fingerprints [13, 6], or eyes in face images [17]. Magnitudes I_{20} and I_{11} encode the evidence/certainty of the sought symmetry in a local image neighborhood (found by the local maxima of $|I_{20}|$). The beauty of this method is that, apart from a correlation of edge magnitudes, it takes into account the direction of edges. By using complex filters encoding local orientations of the sough pattern, its response is penalized if there is disagreement of local orientations of the image with those of the filter. This is achieved because $c(p)$, as defined in Equation 1, encodes the opposite direction of the sought pattern, so if the image and filter orientations "agree", they are canceled during the complex convolution (thus, the zero argument expected in I_{20}).

This is not exploited by other edge-based detection methods such as the Circular Hough Transform or the Integro-Differential operator, where all boundary pixels contribute equally to (do not penalize) the detection of circles. Indeed, the Generalized Structure Tensor can be seen as a (Generalized) Hough Transform with the additional capability of recognize anti-targets *during* the target recognition [1].

3. Proposed System

We propose the use of the GST for iris segmentation following the process described next (summarized in Figures 2 and 3). After segmentation, we obtain the centre/radius of the two circles that approximates the iris boundaries, and the coordinates of the four cross points (if exist) between the eyelids and the sclera boundary. We also compute the straight line that crosses the upper/lower pair of cross points, so regions above/below are discarded.

3.1. Specularities Removal, Coarse Pupil Detection

Removing reflections is fundamental to detect iris boundaries, especially when reflections are close to them. This is done by filling holes (areas of dark pixels surrounded by lighter pixels) in the complement of the gray-scale image. The intensity of pixels in holes is linearly interpolated from valid neighbors, and this is repeated until all pixels are interpolated. The pupil area is then estimated by thresholding, since the pupil is generally darker than surrounding areas. For better accuracy, histogram equalization is carried out, so dark pixels are mapped to the lowest regions of the histogram. The whole process is shown in Figure 2.

3.2. Localization of Iris Boundaries

This task is done as depicted in Figure 3 (top). We first search for the pupil boundary because it is more likely to be visible than the sclera boundary in the case of eyelids occlusion. For this purpose, we use a circular filter of variable radius. The range of radii is 15-70 pixels for the CASIA database. For each radius, the maximum magnitude of I_{20} is recorded, and the image position where it occurs. Maxima detection is only done in pixels of the pupil area estimated in Section 3.1. A peak in $|I_{20}|$ will be obtained when the radius of the circular filter fits that of the pupil boundary (Figure 3, top left). When it happens, $|I_{20}|$ shows high values only in a small neighborhood around the pupil centre, as observed in Figure 3, bottom left. To improve detection, and to discard spurious peaks, a threshold to the argument of I_{20} is also imposed (+/-3 degrees in this work).

After pupil boundary detection, we search for the sclera boundary. The minimum radius of this filter is dynamically adjusted depending on the pupil radius, and the maximum is set to 140 for the CASIA database. To make the sclera detection more accurate, we define a region where its center will be situated (here we use the whole pupil as candidate region). Although the pupil and sclera circles are not concentric, the fact that the pupil is fully contained within the iris can be used to aid in the sclera search [5]. In addition, to avoid possible occlusion by eyelids and eyelashes, we use a circular filter with the upper and lower regions removed (see Figure 1). As before, the highest response of $|I_{20}|$ is obtained when the radius of the filter fits that of the sclera boundary. A threshold to the argument of I_{20} is also imposed here. When the two radii match, the response of I_{20} is not so concentrated (Figure 3, bottom right). This is probably due to the presence of eyelids/eyelashes that introduce strong edges with random directions in the neighborhood of the sclera boundary. These strong edges are detected by the filter even when it is positioned at a certain distance of the sclera center. The fact that I_{20} does not have zero argument (red color) in these points supports the statement of random edges within the filter spatial band.

3.3. Eyelids occlusion detection

Finally, to detect the cross points between the eyelids and the sclera boundary, we sample the (complex) values of $p = I_{20}/I_{11}$ across the sclera boundary with angle increments of 3 degrees, obtaining 120 samples in the 0-360 range. Given the vector $\mathbf{p} = (p_1, ..., p_i, ..., p_{120})$, we compute for each sample p_i the (real) value $p_i' = \langle p_i - \bar{\mathbf{p}}, p_i - \bar{\mathbf{p}} \rangle$, with $\bar{\mathbf{p}}$ being the mean of $\mathbf{p}$. The resulting vector $\mathbf{p}' = (p_1', ..., p_i', ..., p_{120}')$ can be seen in Figure 3 (top), third plot. As observed, regions with no occlusion have small variance. The transition to regions of high variance is used to detect the 4 cross points between the eyelids and the sclera (in case of low variance in an entire quadrant, we determine that there is no occlusion). This is because we expect that in regions without occlusion, the Schwartz inequality between $|I_{20}|$ and I_{11} will tend to equality. Therefore, the ratio $|I_{20}|/I_{11}$ will tend to one. On the other hand, in occluded regions, the Schwartz inequality will not hold, and $|I_{20}|/I_{11}$ will have an erratic behavior, with high variance.

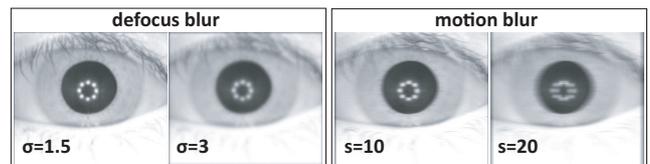| defocus blur		motion blur	
σ=1.5	σ=3	s=10	s=20

Figure 4. Example of synthetic degradations applied to the image of Figure 1.

4. Experimental Framework

4.1. Database and Baseline Systems

We use the CASIA-IrisV3-Interval database [3], with 2,655 images of 280×320 pixels from 249 contributors acquired in 2 sessions. Images per contributor and per session
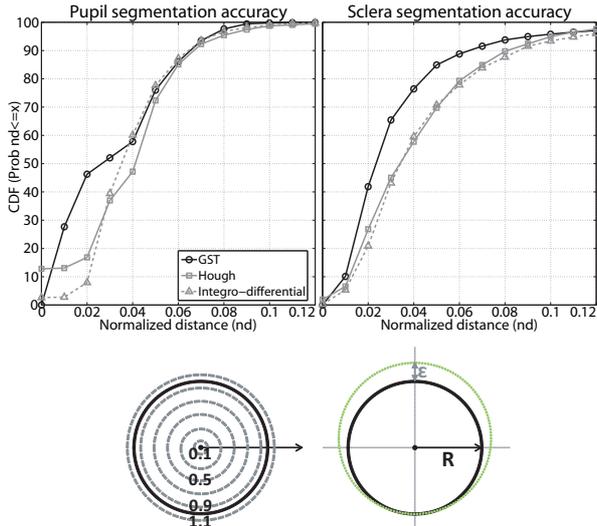
Figure 5. Top: Segmentation accuracy without image perturbations. Bottom left: relative distance in terms of the radius of the circle. Bottom right: detection accuracy in terms of maximum offset ϵ with respect to the annotated circle. The offset ϵ is normalized by the radius R of the annotated circle for size and dilation invariance.

are not constant and not all the individuals have images of the two eyes. The number of different eyes is 396. A development set of 50 subjects (comprising 489 images) and a test set of 199 subjects (2166 images) are defined in this work. The development set has been used to find the optimal configuration of our segmentation system described in Section 3, whereas the test set is used for validation.

We compare our method to the two most widely used algorithms for iris boundary detection based on the circular Hough transform [18] and the Daugman integro-differential operator [4]. For this purpose, we have used two publicly available implementations [1]. The baseline matcher used is also included in the Libor Masek source code. The iris region is unwrapped to a normalized rectangle using the Daugman's rubber sheet model [4] and next, a 1D Log-Gabor wavelet is applied plus phase binary quantization. Matching is done using the normalized Hamming distance, so only significant (non-noisy) bits are used. Hamming scores are further normalized to compensate for different number of bit pairs available for comparison [5].

4.2. Synthetic Perturbations

Several quality factors can degrade iris recognition performance [10], like image blur, off-angle, occlusion, resolution, lightning variation or reflections. Successful iris segmentation has a major influence on the performance of any subsequent analysis algorithm, so it is of utmost importance

---

[1]Hough: implementation by Libor Masek. Integro-differential: implementation by Anirudh Sivaraman (http://web.mit.edu/anirudh/www)
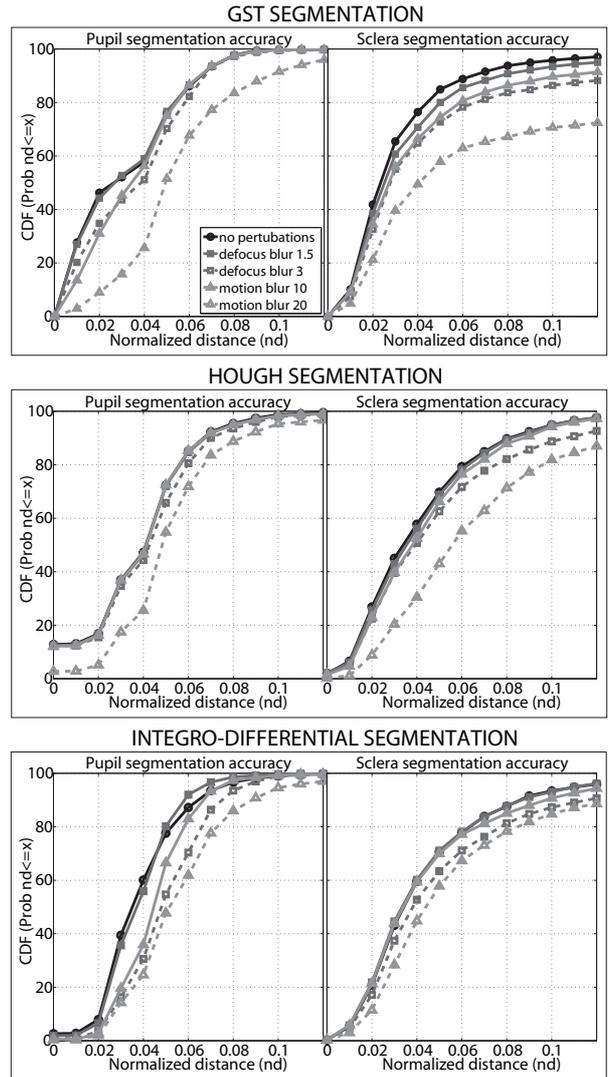

Figure 6. Segmentation accuracy with image perturbations.

to evaluate the effects of quality factors on the segmentation. Here we use synthetically degraded images, inspired by the study [9]. CASIA-IrisV3-Interval is a database of good quality close-up indoor images, with very clear texture details. Starting with good quality images, we apply different degradations. We concentrate on image blur caused by defocus and by motion. An example of synthetically degraded images is shown in Figure 4.

Defocus blur mostly occurrs when the focal point is outside the depth of field (DOF) of the captured object. DOF is affected by aperture size or zooming of the camera. In iris images, DOF is in the range of centimeters due to the required aperture in close-up acquisition or the zooming needed at higher distances [18, 12]. DOF is the distance that the head of the subject is allowed to move to/from the camera before the image is defocused. Thus, it is a key factor

in iris acquisition, typically overcome by video acquisition and best frame selection, but depending on the scenario, it is not guaranteed that clear, sharp images are available. To simulate defocus blur, we convolve the image with a low-pass Gaussian filter of variable standard deviation.

Motion blur results from the relative object/camera movement, because any (or both) of them are in movement. There are two types of motion blur, linear and non-linear. Linear motion can be modeled as "smearing" in only one direction, while non-linear involves smearing in multiple directions with different strengths. Here we consider only linear motion blur, simulated with two parameters: direction of smear (angle) and amount of pixel-smear (strength). The strength corresponds to the length of the blur in pixels. In our study, the angle is set to zero (motion blur along the horizontal axis). This is the most adverse condition for our database. When there are eyelids partially occluding the image (as in Figure 4), sclera boundaries have mostly vertical directions. Therefore, motion blur in perpendicular direction will have the highest impact in these boundaries.

4.3. Results

In Figure 5 (top), we give the performance of our segmentator and of the baseline segmentators. We have manually annotated the database images, computing the radius and the center of the iris and sclera circles. Segmentation accuracy is evaluated by the maximum offset ϵ of the detected circle with respect to the annotated one [19]. The offset is normalized by the radius of the annotated circle for size and dilation invariance, as shown in Figure 5 (bottom).

We observe in Figure 5 that the proposed algorithm works better than the two baseline systems. Detected pupil and sclera circles using the GST are closer to the annotated circles, which is more evident in the detection of the sclera. It is also observed that sclera detection gives worse performance than pupil detection (nearly 100% of the pupils are segmented with an error below 9-10%, whereas 90-95% of the scleras are segmented with this same error).

Figure 6 gives the performance of the three segmentators with different degrees of image degradation. For better system comparison, we plot in Figure 7 the comparative performance for a segmentation error of 5% or less (nd=0.05 in the x-axes of Figure 6). A number of interesting findings can be observed. Concerning pupil detection, the GST and Hough algorithms are not too much affected by any level of defocus, nor by small levels of motion blur. Only high amounts of motion blur have significant impact in their performance. On the other hand, the Integro-differential algorithm is affected by all perturbations (except low levels of defocus). Concerning sclera detection, the GST algorithm is affected by all perturbations, especially under severe motion blur. Their two counterparts significantly degrade only under severe levels of defocus or motion blur. Despite this,

the GST is always the best sclera detector (or in the top) for nearly all perturbation levels, according to Figure 7. To sum up, comparatively, the GST algorithm is always on top, with similar performance than the others in pupil detection, and clearly better for sclera detection.

To evaluate the eyelids detection, we give in Figure 8 recognition results with and without incorporating this stage (using non-degraded images only). Intra-class experiments are done by matching all iris images of the same eye between them (avoiding symmetric matches). Inter-class experiments are done by matching the first available image of a given eye with the second image of all the remaining eyes in the database. This results in 6,810 genuine and 95,772 impostor scores. An improvement in performance is observed across the whole DET when including the eyelids removal step. Also, it results in a FRR decrease for any given value of the Hamming distance, and a shifting of the inter-class distance distribution towards smaller values, thus pointing out the validity of our eyelid removal algorithm.
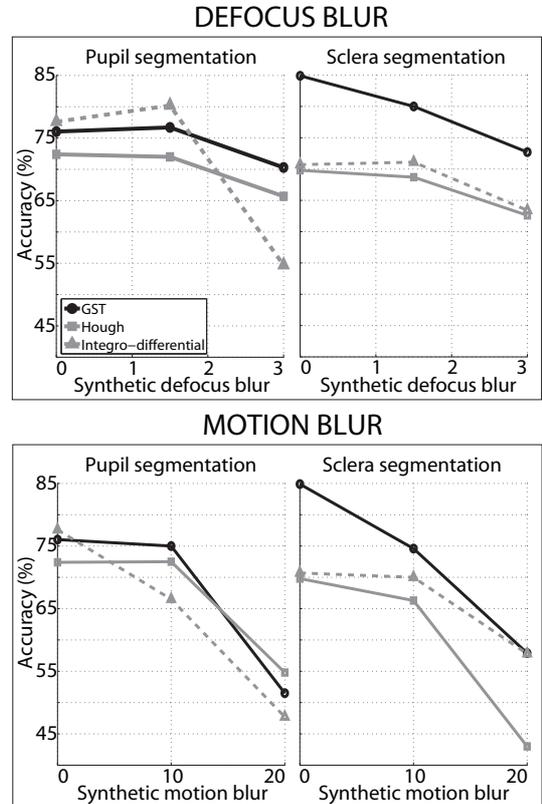

Figure 7. Segmentation accuracy with image perturbations. Accuracy values correspond to a segmentation error of 5% or less (nd=0.05 in the x-axes of Figure 6).

5. Conclusions

An iris segmentation algorithm using the Generalized Structure Tensor (GST) has been proposed. We first search

for the pupil boundary using a circular filter of variable radius. A second circular filter with the upper and lower regions removed is then used for sclera detection. We employ this sequential procedure since the pupil is more likely to be visible in the case of occlusion. Eyelid area is also computed by finding the cross position between the eyelids and the sclera boundary. We compare our system with popular segmentation algorithms based on circular Hough transform and integro-differential operators. Contrarily to these two approaches, the GST uses complex filters encoding local orientations, so its response is penalized if there is disagreement of local image orientations with those of the filter [1]. As a result, our system outperforms the baseline systems in several of the scenarios evaluated.
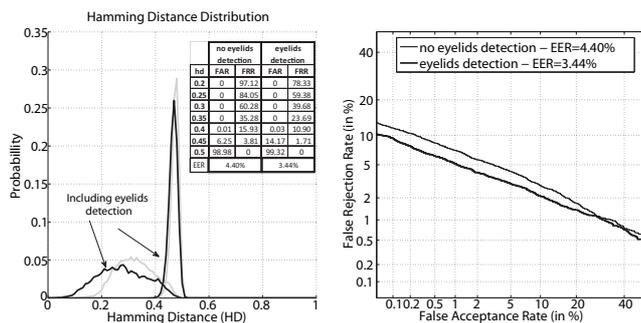

Figure 8. Left: Inter- and intra-class Hamming distance distribution with and without eyelids detection. Right: DET curves. False Accept and False Reject Rates (FAR, FRR) at different working points are given, as well as the Equal Error Rate (EER).

Using manual segmentation as benchmark for our experiments, we observe that the GST algorithm works better than their counterparts. This is more evident in detecting the sclera, where the GST gets much better accuracy. Also, in general, pupil is detected more accurately than sclera with any given system. One reason could be the occlusion of eyelids and eyelashes, since the database used is mostly of oriental people. In addition, verification results of the proposed system using 1D Log-Gabor wavelets show an improvement in performance when including the eyelid removal step. These results show the validity of our proposed approach and demonstrate that the Generalized Structure Tensor constitutes an alternative to classic iris segmentation approaches. Although our approach make use of circular filters, certain degree of non-circularity can be accommodated by controlling the width of the filter, so once approximate circular boundaries are detected, they can be deformed into non-round boundaries. This idea is followed by most recent segmentation approaches [5, 7, 8] and even algorithms not relying initially on geometric models for detection [15] also make use of some circular or elliptical fitting during a refinement stage. We also evaluate the influence of different degrees of image defocus and motion blur in the segmentation performance. These degradations can be found not only in distant or uncontrolled acquisition, but also in close-up images. Comparatively, our GST algorithm always gets top performance for all levels of degradation, with similar performance than the others in pupil detection, and clearly better performance for sclera detection.

Future work includes improving eyelids localization and including eyelashes detection. Eyelids can be modeled as circles, so the algorithm presented in this paper can also be used for accurately finding its position. We will also evaluate the GST under other degradations found in less cooperative environments, e.g. lightning variation, noise and resolution. The robustness of our system to off-axis images will also be assessed. These environments are one of the hottest research topics in biometrics [12, 14], which drastically reduces the need of user's cooperation, and will be an important source of future work.

Acknowledgements

References

[1] J. Bigun. *Vision with Direction*. Springer, 2006.

[2] J. Bigun, G. Granlund, J. Wiklund. Multidimensional orientation estimation with applications to texture analysis and optical flow. *IEEE TPAMI*, 13(8), 1991.

[3] CASIA Iris Image Database. http://biometrics.idealtest.org.

[4] J. Daugman. How iris recognition works. *IEEE TCSVT*, 14:21–30, 2004.

[5] J. Daugman. New methods in iris recognition. *IEEE TSMC-B*, 37(5), 2007.

[6] H. Fronthaler, K. Kollreider, J. Bigun, J. Fierrez, F. Alonso-Fernandez, J. Ortega-Garcia, J. Gonzalez-Rodriguez. Fingerprint Image Quality Estimation and its Application to Multi-Algorithm Verification. *IEEE TIFS*, 3(2), 2008.

[7] Z. He, T. Tan, Z. Sun, X. Qiu. Toward accurate and fast iris segmentation for iris biometrics. *IEEE TPAMI*, 31(9):1295–1307, 2010.

[8] D. Jeong, J. Hwang, B. Kang, K. Park, C. Won, D.-K. Park, J. Kim. A new iris segmentation method for non-ideal iris images. *IVC*, 28(2):254–260, 2010.

[9] N. Kalka, V. Dorairaj, Y. Shah, N. Schmid, B. Cukic. Image Quality Assessment for Iris Biometric. *Proc. BCC*, 2005.

[10] N. D. Kalka, J. Zuo, N. A. Schmid, B. Cukic. Estimating and Fusing Quality Factors for Iris Biometric Images. *IEEE TSMC-A*, 40(3):509–524, 2010.

[11] L. Ma, T. Tan, Y. Wang, D. Zhang, "Efficient iris recognition by characterizing key local variations," *IEEE TIP*, 13(6), 2004.

[12] J. Matey, O. Naroditsky, K. Hanna, R. Kolczynski, D. LoIacono, S. Mangru, M. Tinker, T. Zappia, W. Zhao. Iris on the move: acquisition of images for iris recognition in less constrained environments. *Proc. IEEE*, 94(11), 2006.

[13] K. Nilsson, J. Bigun. Localization of corresponding points in fingerprints by complex filtering. *Pattern Recognition Letters*, 24:2135–2144, 2003.

[14] NIST MBE, *Multiple Biometrics Evaluation - http://face.nist.gov/mbe*, 2009.

[15] S. Pundlik, S. Birchfield, D. Woodard. Iris segmentation in non-ideal images using graph cuts. *IVC*, 28(12):1671–1681, 2010.

[16] E. Tabassi, P. Grother, and W. Salamon, "IREX II - IQCE - iris quality calibration and evaluation. performance of iris image quality assessment algorithms," *NISTIR 7296 - http://iris.nist.gov/irex/*, 2011.

[17] D. Teferi, J. Bigun. Multi-view and multi-scale recognition of symmetric patterns. *Proc. SCIA*, LNCS-5575:657–666, 2009.

[18] R. P. Wildes. Iris recognition: An emerging biometric technology. *Proc. IEEE*, 85(9):1348–1363, 1997.

[19] J. Zuo, N. Schmid. An automatic algorithm for evaluating the precision of iris segmentation. *Proc. BTAS*, 2008.